nature physics

LETTERS

PUBLISHED ONLINE: 18 JULY 2016 | DOI: 10.1038/NPHYS3831

Large anomalous Hall effect in a half-Heusler antiferromagnet

T. Suzuki[1], R. Chisnell[2], A. Devarakonda[1], Y.-T. Liu[1], W. Feng[3], D. Xiao[4], J. W. Lynn[2] and J. G. Checkelsky[1]*

The quantum mechanical (Berry) phase of the electronic wavefunction plays a critical role in the anomalous[1,2] and spin Hall effects[3,4], including their quantized limits[5–7]. While progress has been made in understanding these effects in ferromagnets[8], less is known in antiferromagnetic systems. Here we present a study of antiferromagnet GdPtBi, whose electronic structure is similar to that of the topologically non-trivial HgTe (refs 9–11), and where the Gd ions offer the possibility to tune the Berry phase via control of the spin texture. We show that this system supports an anomalous Hall angle $\Theta_{AH} > 0.1$, comparable to the largest observed in bulk ferromagnets[12] and significantly larger than in other antiferromagnets[13]. Neutron scattering measurements and electronic structure calculations suggest that this effect originates from avoided crossing or Weyl points that develop near the Fermi level due to a breaking of combined time-reversal and lattice symmetries. Berry phase effects associated with such symmetry breaking have recently been explored in kagome networks[14–17]; our results extend this to half-Heusler systems with non-trivial band topology. The magnetic textures indicated here may also provide pathways towards realizing the topological insulating and semimetallic states[9–11,18,19] predicted in this material class.

The ordinary Hall effect is due to the Lorentz force bending of charge carriers perpendicular to a magnetic field. In systems where time-reversal symmetry (TRS) is spontaneously broken, it typically can be overwhelmed by a different class of mechanisms for transverse velocity. In such systems, there are contributions to transverse velocity from both extrinsic effects due to spin-dependent scattering[13] and intrinsic effects related to real space[20,21] and momentum space[2] Berry phase mechanisms. The former is relevant in systems with non-coplanar spin textures with finite scalar spin chirality $\chi_{ijk} = \boldsymbol{S}_i \cdot (\boldsymbol{S}_j \times \boldsymbol{S}_k)$, where $\boldsymbol{S}_n$ are spins, while the latter generically occurs in TRS-broken systems originating from the spin–orbit-interaction-induced Berry curvature of the filled bands. The anomalous Hall effect (AHE) due to magnetic texture is most often associated with finite χ_{ijk} and tends to exhibit relatively small anomalous Hall angles $\Theta_{AH} \lesssim 0.01$ (such as $SrFeO_3$ (ref. 22) or $Pr_2Ir_2O_7$ (ref. 23)), while intrinsic band-structure-based effects are common in ferromagnetic systems and can be significantly larger[13]. Recent theoretical work has suggested that effects that rely on both magnetic texture and strong spin–orbit coupling may exist in non-collinear antiferromagnets that lead to significant Hall responses[14]. Single-crystal studies of Mn_3Sn and Mn_3Ge have been shown to support $\Theta_{AH} \lesssim 0.02$ and 0.05, respectively, originating from its inverse triangular spin structure and electronic structure[16,17].

Here we study single crystals of GdPtBi, a member of the family RPtBi (R is a rare earth element) known to exhibit antiferromagnetic ordering[24]. As shown in Fig. 1a, this system has the half-Heusler structure consisting of interpenetrating face centred cubic (fcc) lattices of each constituent element (space group $F\bar{4}3m$) with lattice constant $a = 6.68$ Å for R = Gd. In general, the antiferromagnetic fcc lattice is frustrated, with the Gd ions forming a triangular lattice when viewed along the $\langle 111 \rangle$ direction. From the high-temperature magnetic susceptibility we find a Curie–Weiss temperature $\theta_{CW} = -38$ K, while the transition to long-range magnetic order occurs at $T_N = 9.2$ K, as shown in Fig. 1b, consistent with previous reports[24]. This yields a moderate frustration parameter $f \equiv -\theta_{CW}/T_N \sim 4$, similar to insulating fcc systems FeO and MnSe[25]. As shown in Fig. 1c, high-field torque magnetometry reveals a distinct kink at a magnetic field $B_C \approx 25$ T (seen more clearly in $d^2\tau/dB^2$, which is proportional to the magnetic susceptibility), which is independent of orientation, as shown in the inset of Fig. 1c. This is suggestive of field-induced alignment of the spins and an energy scale $g\mu_B SB_C = 120$ K, where $g = 2$ is the g-factor, μ_B is the Bohr magneton, and $S = 7/2$ is the Gd spin (see Supplementary Information). This is approximately three times larger than θ_{CW}, indicating cancelling exchange interactions, as has been theoretically discussed for this material[26]. The structure of the magnetic ordering in $B = 0$ has recently been probed by X-ray and neutron scattering, which suggests an antiferromagnetic ordering (type-II) in which the Gd moments order ferromagnetically in sheets in the (111) planes, which in turn are stacked antiferromagnetically[27]. Theoretical work has suggested that other orderings are of comparable energy[26]; the structure at finite B has not been previously reported.

The focus of the present study is the interplay of the magnetic structure and strong spin–orbit coupling in GdPtBi. The heavy-element PtBi sublattice is expected to provide the system with a similar electronic structure to that of HgTe (refs 9–11), sensitive to the magnetic ordering of the Gd ions through the spin–orbit interaction. The bulk electronic structure of GdPtBi is known to be semimetallic[28]. As shown in Fig. 1b, the observed resistivity as a function of temperature $\rho(T)$ has a moderate increase with decreasing T, while at low temperature it shows a clear kink concomitant with the magnetic transition at T_N. A richer perspective of the coupling of the conduction electrons to the magnetic order is provided by magnetotransport. The longitudinal resistivity as a function of magnetic field $\rho_{xx}(B)$, with B along the [001] direction, is shown in Fig. 2a. At temperatures $T > T_N$ we observe an approximately quadratic dependence on B, indicating an average mobility $\mu_{avg} \approx 1{,}000\ cm^2\ V^{-1}\ s^{-1}$. As T is lowered, we observe

[1]Department of Physics, Massachusetts Institute of Technology, Cambridge, Massachusetts 02139, USA. [2]NIST Center for Neutron Research, National Institute of Standards and Technology, Gaithersburg, Maryland 20899, USA. [3]School of Physics, Beijing Institute of Technology, Beijing 100081, China. [4]Department of Physics, Carnegie Mellon University, Pittsburgh, Pennsylvania 15213, USA. *e-mail: checkelsky@mit.edu

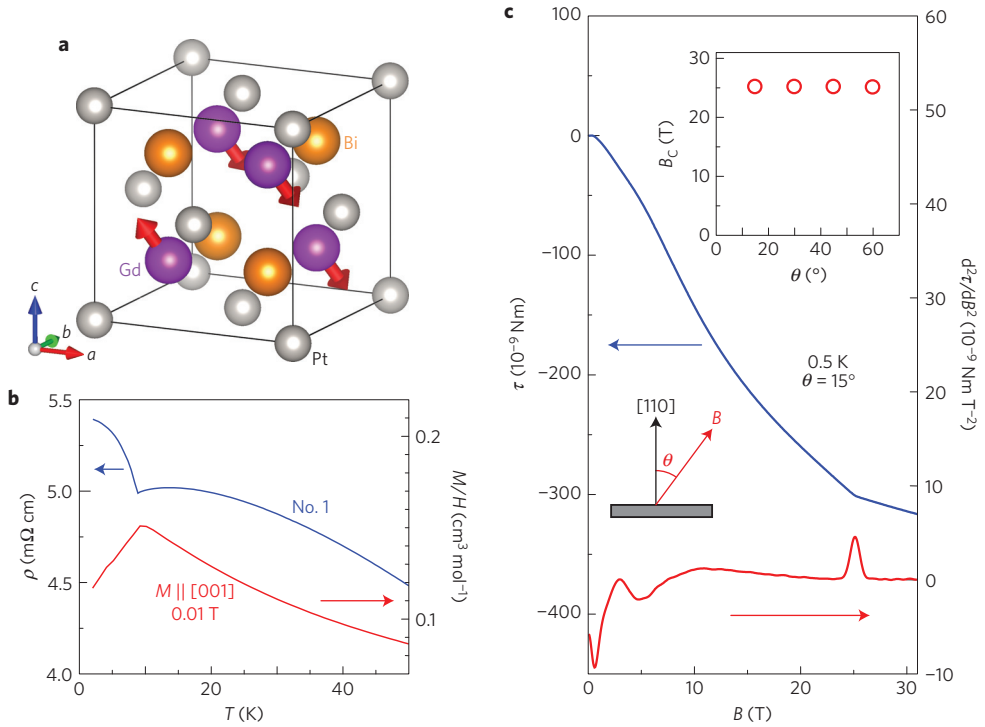

Figure 1 | Magnetic ordering in GdPtBi. a, Crystal structure of GdPtBi, consisting of three interpenetrating fcc lattices with lattice constant $a = 6.68$ Å. The spin direction for Gd in the antiferromagnetic phase is shown. **b**, Resistivity ρ and magnetic susceptibility M/H for a magnetic field B along the [001] direction as a function of temperature T through the antiferromagnetic transition temperature $T_N = 9.2$ K. $B = 0.01$ T is applied for the measurement of M/H. **c**, Magnetic torque measured to $B = 31$ T (blue line). The geometry of field and crystal is shown in the inset. The second derivative $d^2\tau/dB^2$ (also shown in main panel, red line) shows a sharp change near $B = 25$ T that is independent of orientation (shown in the upper inset).

a dip in ρ_{xx} that develops near $B = 4$ T, progressively deepening to $T = 2.5$ K. Measurements to $B = 31$ T (see Supplementary Information) show that this is not related to Landau quantization, as no continued pattern in B^{-1} connected to this feature is observed with the appearance of Shubnikov–de Haas (SdH) oscillations for $B > 10$ T.

The field dependence of the transverse resistivity $\rho_{yx}(B)$ is shown in Fig. 2b. At $T = 50$ K we see a Hall effect consistent with multiband conduction, as would be expected from the electronic structure[28]. Upon lowering T, we see a prominent feature develop in the vicinity of $B = 4$ T, which corresponds to an enhancement in ρ_{yx} of 55% at $T = 2.5$ K. This feature draws a distinct contrast with the magnetization M. As shown in Fig. 2c, for T both above and below T_N, we see an approximately linear and featureless $M(B)$. In magnetic systems, it is conventional to describe three separate contributions to $\rho_{yx} = R_0 B + R_S M + \rho_{yx}^T$, where R_0 is the ordinary Hall coefficient, R_S is the anomalous Hall coefficient coupled to M, and ρ_{yx}^T is the Hall effect arising from spin textures. As described above, the final among these include non-coplanar textures that generate finite χ_{ijk} (refs 29–31) as well as non-collinear textures that allow finite momentum-space Berry curvature[14–17]. Structure in $\rho_{yx}(B)$ from Berry phase effects normally mirrors that in M unless there are contributions related to spin texture. Mathematical separation of these components is often performed in the literature to isolate ρ_{yx}^T (ref. 32). Performing such analysis we estimate $\rho_{yx}^T = 0.18$ mΩ cm (see Supplementary Information), significantly larger than has been previously reported in any antiferromagnetic system, both in terms of absolute value and size relative to ρ_{xx} (see Supplementary Information). We note that the empirical relationship used for additivity of the contributions to ρ_{yx} is valid only in the limit of small Hall angle, whereas at all values of the Hall angle it is possible to discuss additivity in the transverse conductivity σ_{xy}. Here we quantify the AHE using the anomalous Hall angle $\Theta_{AH} = \sigma_{xy}^A/\sigma_{xx} = (\sigma_{xy} - \sigma_{xy}^N)/\sigma_{xx}$, where A(N) denotes the anomalous (normal) part of the Hall conductivity. We estimate σ_{xy}^N by using $\sigma_{xy}(T = 50\ \mathrm{K})$, which is far above T_N and reflects the ordinary contribution to the Hall effect, and refer to the resulting anomalous Hall contribution as $\Delta\sigma_{xy}$, as shown in Fig. 2e (similar behaviour is obtained by fitting the σ_{xy}^N at large B). The value of Θ_{AH} peaks at more than 0.15 at $B = 4$ T, which is larger than has been previously observed in antiferromagnetic systems. A view of this transport response in the space of B and T is shown in Fig. 3a. The region with the largest $\Delta\sigma_{xy}$, corresponding to the peak feature we observe, occurs near $B = 4$ T and below $T_N = 9.2$ K. However, the anomalous Hall response persists to significantly higher temperatures, with a reduced magnitude, finally disappearing between 25 and 30 K.

The most common contribution of magnetic texture to the AHE is that of finite χ_{ijk} appearing in systems that have skyrmionic spin textures stabilized by the Dzyaloshinskii–Moriya interaction[30,31]. It has also been recognized that frustrated magnets may play host to similar texture-induced Hall effects[23]. More recently, theoretical work has suggested that, in antiferromagnets, a band-structure-induced intrinsic AHE may arise in the presence of non-collinear spin structures that break the combined time-reversal and lattice symmetries of the simple antiferromagnetic state[14]. Such a situation is realized in GdPtBi as the $B = 0$ type-II antiferromagnetic spin structure cants in finite B. Neutron scattering measurements confirm both the type-II ordering in fields up to 10 T (see Supplementary Information) and a ferromagnetic canting, as evidenced by an increase in intensity at the nuclear Bragg positions with increasing B, as shown for (111) in Fig. 2d along with its scaling with M^2. Additionally, an applied field produces an enhancement in the magnetic Bragg peaks, as shown for (0.5 0.5 2.5) in Fig. 2d, which saturates above 6 T, similar to the field scale for disappearance of the anomalous Hall response. For antiferromagnetic systems

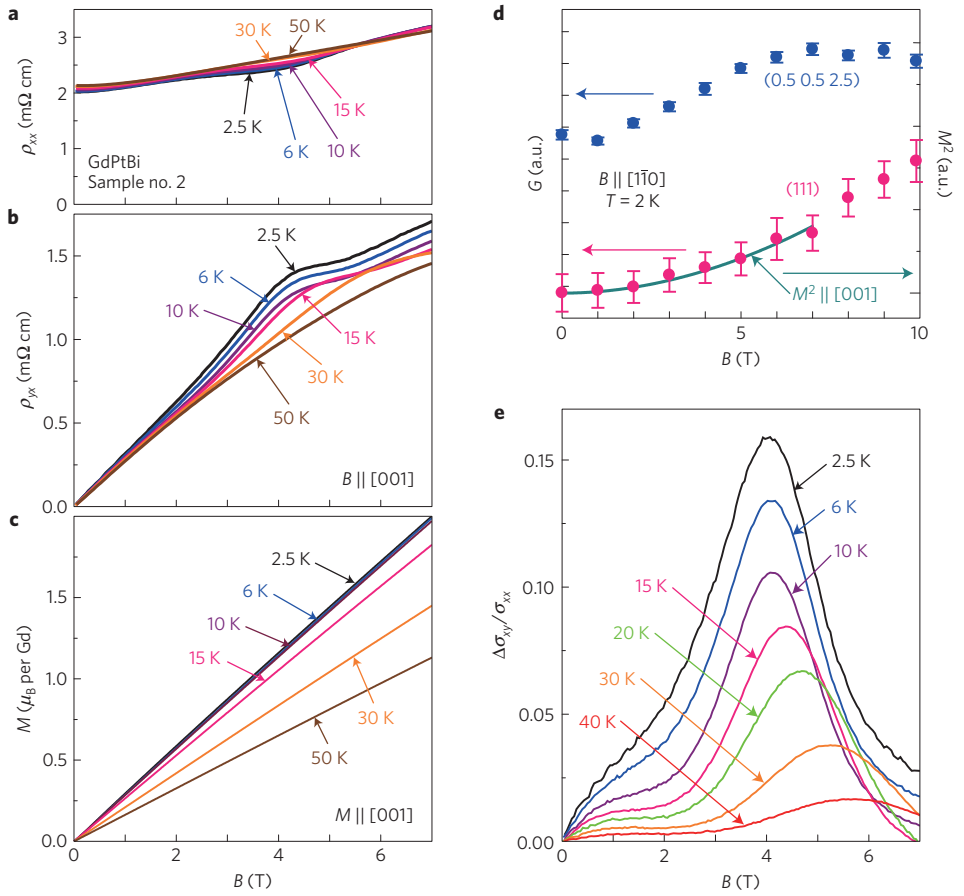

Figure 2 | Magnetotransport in GdPtBi. a, Longitudinal resistivity as a function of B along [001]. **b**, Transverse resistivity as a function of B along [001]. **c**, Magnetization as a function of B along [001]. **d**, Integrated Gaussian area G of (0.5 0.5 2.5) and (111) Bragg peaks, proportional to the square of the sublattice magnetization and bulk magnetization, respectively, measured using neutron scattering as a function of B applied along [1$\bar{1}$0] at $T = 2$ K. The square of M at $T = 2$ K is also plotted. Error bars indicate the standard error. **e**, Anomalous Hall angle $\Delta\sigma_{xy}/\sigma_{xx}$ as a function of temperature.

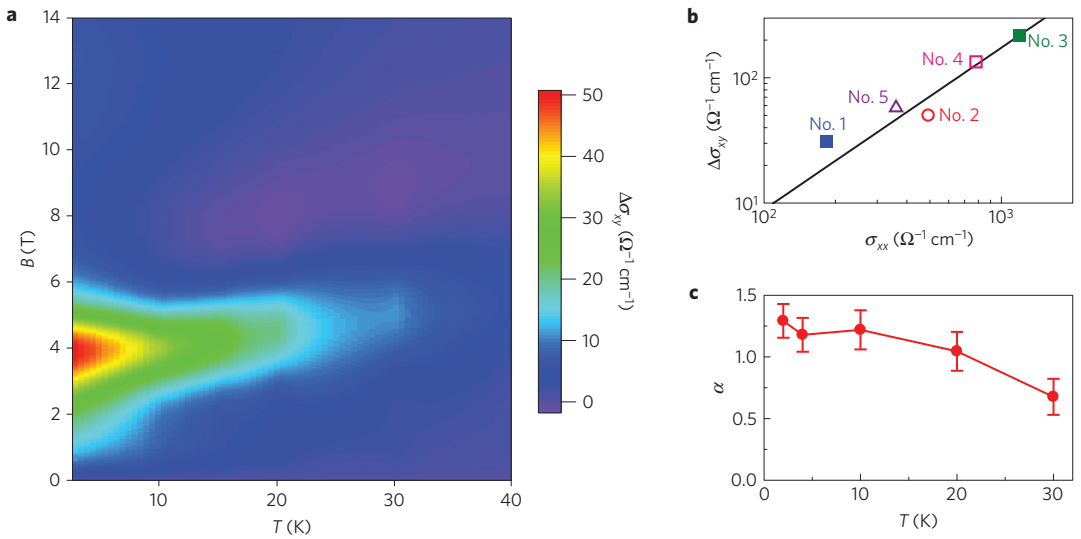

Figure 3 | Anomalous Hall response of GdPtBi. a, Colour plot of $\Delta\sigma_{xy}$ for T between 2 K and 50 K and B from 0 to 14 T. **b**, Scaling of the anomalous Hall conductivity $\Delta\sigma_{xy}$ as a function of σ_{xx} for five different single crystals. The straight line is a fit to the power-law $\Delta\sigma_{xy} \propto \sigma_{xx}^{\alpha}$. **c**, Temperature dependence of the scaling power-law α. Error bars indicate the standard error.

with such broken time-reversal and lattice symmetries and large spin–orbit coupling, the anomalous Hall response is predicted to be significant—calculated to be 218 Ω^{-1} cm^{-1} for Mn_3Ir (ref. 14). The variation of the Hall response across five different GdPtBi crystals is shown in Fig. 3b; the observed $\Delta\sigma_{xy} = 30$–$200\ \Omega^{-1}$ cm^{-1} are comparable to that predicted for the intrinsic AHE case. We note that the transport observations also parallel predictions for the distorted fcc lattice with finite orbital magnetization[33]. However,

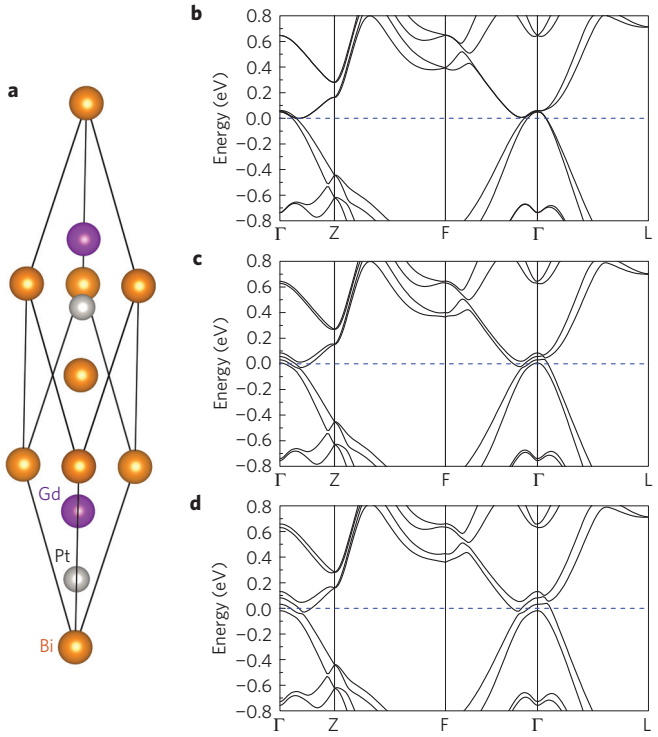

Figure 4 | Electronic structure of magnetically ordered GdPtBi. **a**, Rhombohedral magnetic unit cell for type-II magnetically ordered GdPtBi. **b**, Electronic structure without an external magnetic field. **c**,**d**, Electronic structure for canted type-II magnetic order in the presence of applied magnetic fields $B = 4$ T and 8 T, respectively, applied along the [001] direction.

this requires the presence of a type-I magnetic ordering and finite χ_{ijk}, which is inconsistent with our neutron scattering measurements (see Supplementary Information).

In terms of scaling of the AHE, we find a temperature-dependent scaling factor α (defined as $\Delta\sigma_{xy} \sim \sigma_{xx}^{\alpha}$), as shown in Fig. 3c. At low T, we find $\alpha = 1.2$, intermediate between the value of 1.6 expected for the intrinsic AHE in multiband disordered metals[34,35] and the σ_{xx}-invariant intrinsic AHE in moderately clean systems. This crossover is predicted to occur in ferromagnets in the vicinity of $\sigma_{xx} \sim 10^3\ \Omega^{-1}\,\mathrm{cm}^{-1}$, similar to the scale observed here. The existence of frustrated magnetic interactions in GdPtBi, as shown by the moderate value of f, suggests that short-range correlations persist above T_N (ref. 26); such correlations in the absence of long-range order have been shown to affect transport in $PdCrO_2$ (ref. 36) and $Pr_2Ir_2O_7$ (ref. 23). We hypothesize that this extends to the anomalous Hall effect observed here, as such fluctuations will break the same symmetry as the ordered phase, which is distinct from that expected for Mn_3Ge and Mn_3Sn, where fluctuations due to symmetric exchange cancel (see Supplementary Information).

To investigate the origin of the large AHE allowed in GdPtBi in finite B, we consider the effect of the spin texture on the electronic structure. Band-touching points in the bulk electronic structure of GdPtBi have been previously reported in calculations with an uncanted magnetic structure[37] which, if driven to anticrossings near the Fermi level, could be a source of significant AHE as in ferromagnetic systems[35]. We have performed electronic structure calculations for magnetically ordered GdPtBi using the rhombohedral magnetic unit cell shown in Fig. 4a. The approximate location of E_F is determined from the ordinary Hall effect and k_F from SdH oscillations (see Supplementary Information), and the B dependence of the spin structure is calculated using the results of the magnetic and neutron scattering experiments. For $B = 0$ we find that the type-II ordered system exhibits band touching at Γ, as shown in Fig. 4b. The structures with spin canting for $B = 4$ T and 8 T along the [001] direction are shown in Fig. 4c and d, respectively. The bands near the Fermi level originate from Pt and Bi (see Supplementary Information). The combination of the large spin–orbit coupling and critical band alignment of the system amplifies the physical consequence of the Gd spin texture on these bands; inspection of the band structure shows the development of avoided crossings near E_F which carry significant Berry curvature. This suggests that the evolution of the electronic structure due to spin texture will generate significant Berry phase contributions to the AHE. The requirement that the combined symmetry of the antiferromagnetic state be broken to observe the AHE necessitates the application of finite B (ref. 14)—the calculations here indicate that the particularly large response relies on the detailed band structure of GdPtBi itself. We note that Weyl points have been predicted to appear in the electronic structure of the HgTe class compounds[18], and can be a source of significant anomalous Hall conductivity[15,16,38]. While such points do not appear along the high-symmetry directions in the calculated structure, here they may be expected to appear at other points in momentum space[39]. If sufficiently isolated Weyl points exist near E_F, they may also contribute to the AHE in a manner similar to avoided crossings (magnetotransport possibly indicative of Weyl points is observed in these crystals as shown in the Supplementary Information). Further theoretical work is needed to determine if such conditions are met in GdPtBi. More broadly, the symmetry-allowed momentum-space Berry phase mechanism provides a consistent description for the transport, scattering and calculation results presented herein.

It has been predicted that spin–orbit-driven band inversion in the bulk of RPtBi may give rise to a topological insulating state[9–11], although thus far experiments using photoemission to probe the band structure have been unable to resolve the topological nature of the surface bands[28]. The symmetry-broken ground states known to occur in RPtBi are then of heightened interest, as they would be projected on to a potentially topologically non-trivial ground state. The evolution of the bulk band structure is relevant to the AHE presented here; the band topology of RPtBi provides a band structure acutely sensitive to gap formation via the magnetic texture and strong spin–orbit coupling of the system. Additionally, the antiferromagnetic ordering itself has been predicted to give rise to a new type of topological insulating state where a combined time-reversal and translational symmetry is the source of protection for the surface modes[19], a scenario further enriched by the observations here. This highlights GdPtBi as a candidate platform not only for hosting topological edge modes in the antiferromagnetic state[19], but also as a novel TRS-broken topological insulator with non-collinear spin texture in finite B (ref. 6).

The combination of spin–orbit and correlation effects is expected to reveal new behaviour beyond that possible for single-electron physics. Here, the combination of strong spin–orbit coupling and symmetry breaking probed by neutron scattering gives rise to an extremely large anomalous Hall response that connects to recent theories for emerging effects in antiferromagnetic systems[14] and the calculated electron structure. This effect and its scaling with conductivity[12] provide an antiferromagnetic example to generalize the notion of phase-space Berry phase effects in TRS-broken systems[40]. Furthermore, it provides an example of a robust AHE driven by the combined role of spin–orbit coupling and spin texture that demonstrates the ubiquity of the Berry phase mechanism in symmetry-broken systems.

Methods

Methods, including statements of data availability and any associated accession codes and references, are available in the online version of this paper.

Received 18 January 2016; accepted 16 June 2016; published online 18 July 2016

References

1. Karplus, R. & Luttinger, J. M. Hall effect in ferromagnetics. *Phys. Rev.* **95,** 1154–1160 (1954).
2. Haldane, F. D. M. Berry curvature on the Fermi surface: anomalous Hall effect as a topological Fermi-liquid property. *Phys. Rev. Lett.* **93,** 206602 (2004).
3. Murakami, S., Nagaosa, N. & Zhang, S.-C. Dissipationless quantum spin current at room temperature. *Science* **301,** 1348–1351 (2003).
4. Sinova, J. *et al*. Universal intrinsic spin Hall effect. *Phys. Rev. Lett.* **92,** 126603 (2004).
5. Yu, R. *et al*. Quantized anomalous Hall effect in magnetic topological insulators. *Science* **329,** 61–64 (2010).
6. Nomura, K. & Nagaosa, N. Surface-quantized anomalous Hall current and the magnetoelectric effect in magnetically disordered topological insulators. *Phys. Rev. Lett.* **106,** 166802 (2011).
7. Kane, C. L. & Mele, E. J. Z_2 topological order and the quantum spin Hall effect. *Phys. Rev. Lett.* **95,** 146802 (2005).
8. Xiao, D., Chang, M.-C. & Niu, Q. Berry phase effects on electronic properties. *Rev. Mod. Phys.* **82,** 1959–2007 (2010).
9. Chadov, S. *et al*. Tunable multifunctional topological insulators in ternary Heusler compounds. *Nature Mater.* **9,** 541–545 (2010).
10. Lin, H. *et al*. Half-Heusler ternary compounds as new multifunctional experimental platforms for topological quantum phenomena. *Nature Mater.* **9,** 546–549 (2010).
11. Xiao, D. *et al*. Half-Heusler compounds as a new class of three-dimensional topological insulators. *Phys. Rev. Lett.* **105,** 096404 (2010).
12. Onoda, S., Sugimoto, N. & Nagaosa, N. Quantum transport theory of anomalous electric, thermoelectric, and thermal Hall effects in ferromagnets. *Phys. Rev. B* **77,** 165103 (2008).
13. Nagaosa, N., Sinova, J., Onoda, S., MacDonald, A. H. & Ong, N. P. Anomalous Hall effect. *Rev. Mod. Phys.* **82,** 1539–1592 (2010).
14. Chen, H., Niu, Q. & MacDonald, A. H. Anomalous Hall effect arising from noncollinear antiferromagnetism. *Phys. Rev. Lett.* **112,** 017205 (2014).
15. Kubler, J. & Felser, C. Non-collinear antiferromagnets and the anomalous Hall effect. *Europhys. Lett.* **108,** 67001 (2014).
16. Nakatsuji, S., Kiyohara, N. & Higo, T. Large anomalous Hall effect in a non-collinear antiferromagnet at room temperature. *Nature* **527,** 212–215 (2015).
17. Nayak, A. K. *et al*. Large anomalous Hall effect driven by a nonvanishing Berry curvature in the noncolinear antiferromagnet Mn_3Ge. *Sci. Adv.* **2,** e1501870 (2016).
18. Ruan, J. *et al*. Symmetry-protected ideal Weyl semimetal in HgTe-class materials. *Nature Commun.* **7,** 11136 (2016).
19. Mong, R. S. K., Essin, A. M. & Moore, J. E. Antiferromagnetic topological insulators. *Phys. Rev. B* **81,** 245209 (2010).
20. Ohgushi, K., Murakami, S. & Nagaosa, N. Spin anisotropy and quantum Hall effect in the kagome lattice: chiral spin state based on a ferromagnet. *Phys. Rev. B* **62,** R6065 (2000).
21. Matl, P. *et al*. Hall effect of the colossal magnetoresistance manganite $La_{1-x}Ca_xMnO_3$. *Phys. Rev. B* **57,** 10248–10251 (1998).
22. Ishiwata, S. *et al*. Versatile helimagnetic phases under magnetic fields in cubic perovskite $SrFeO_3$. *Phys. Rev. B* **84,** 054427 (2011).
23. Machida, Y. *et al*. Unconventional anomalous Hall effect enhanced by a noncoplanar spin texture in the frustrated Kondo lattice $Pr_2Ir_2O_7$. *Phys. Rev. Lett.* **98,** 057203 (2007).
24. Canfield, P. C. *et al*. Magnetism and heavy fermion-like behavior in the *R*BiPt series. *J. Appl. Phys.* **70,** 5800–5802 (1991).
25. Ramirez, A. P. Strongly geometrically frustrated magnets. *Annu. Rev. Mater. Sci.* **24,** 453–480 (1994).
26. Khmelevskyi, S. Antiferromagnetic ordering on the frustrated fcc lattice in the intermetallic compound GdPtBi. *Phys. Rev. B* **86,** 104429 (2012).
27. Kreyssig, A. *et al*. Magnetic order in GdBiPt studied by X-ray resonant magnetic scattering. *Phys. Rev. B* **84,** 220408 (2011).
28. Liu, C. *et al*. Metallic surface electronic state in half-Heusler compounds *R*PtBi (*R* = Lu, Dy, Gd). *Phys. Rev. B* **83,** 205133 (2011).
29. Taguchi, Y., Oohara, Y., Yoshizawa, H., Nagaosa, N. & Tokura, Y. Spin chirality, Berry phase, and anomalous Hall effect in a frustrated ferromagnet. *Science* **291,** 2573–2576 (2001).
30. Lee, M., Kang, W., Onose, Y., Tokura, Y. & Ong, N. P. Unusual Hall effect anomaly in MnSi under pressure. *Phys. Rev. Lett.* **102,** 186601 (2009).
31. Neubauer, A. *et al*. Topological Hall effect in the A phase of MnSi. *Phys. Rev. Lett.* **102,** 186602 (2009).
32. Li, Y. *et al*. Robust formation of skyrmions and topological Hall effect anomaly in epitaxial thin films of MnSi. *Phys. Rev. Lett.* **110,** 117202 (2013).
33. Shindou, R. & Nagaosa, N. Orbital ferromagnetism and anomalous Hall effect in antiferromagnets on the distorted fcc lattice. *Phys. Rev. Lett.* **87,** 116801 (2001).
34. Branford, W. R. *et al*. Coexistence of universal and topological anomalous Hall effects in metal CrO_2 thin films in the dirty limit. *Phys. Rev. Lett.* **102,** 227201 (2009).
35. Onoda, S., Sugimoto, N. & Nagaosa, N. Intrinsic versus extrinsic anomalous Hall effect in ferromagnets. *Phys. Rev. Lett.* **97,** 126602 (2006).
36. Daou, R., Fresard, R., Hebert, S. & Maignan, A. Impact of short-range order on transport properties of the two-dimensional metal $PdCrO_2$. *Phys. Rev. B* **92,** 245115 (2015).
37. Li, Z., Su, H., Yang, X. & Zhang, J. Electronic structure of the antiferromagnetic topological insulator candidate GdBiPt. *Phys. Rev. B* **91,** 235128 (2015).
38. Moon, E.-G., Xu, C., Kim, Y. B. & Balents, L. Non-Fermi-liquid and topological states with strong spin–orbit coupling. *Phys. Rev. Lett.* **111,** 206401 (2013).
39. Witczak-Krempa, W. & Kim, Y. B. Topological and magnetic phases of interacting electrons in the pyrochlore iridates. *Phys. Rev. B* **85,** 045124 (2012).
40. Freimuth, F., Bamler, R., Mokrousov, Y. & Rosch, A. Phase-space Berry phases in chiral magnets: Dzyaloshinskii–Moriya interaction and the charge of skyrmions. *Phys. Rev. B* **88,** 214409 (2013).

Acknowledgements

We are grateful to Y. Lee, L. Fu, L. Savary and H. Sakai for fruitful discussions. This research is funded in part by the Gordon and Betty Moore Foundation EPiQS Initiative, Grant GBMF3848 to J.G.C., material development by NSF grant DMR-1554891, and instrumentation development with ARO grant W911NF-16-1-0034. W.F. acknowledges support from the NSF of China (No. 11374033). D.X. acknowledges support from DOE Basic Energy Sciences Grant No. DE-SC0012509. A.D. acknowledges support by the STC Center for Integrated Quantum Materials, NSF Grant No. DMR-1231319. J.G.C. acknowledges support from the Bose Fellows Program at MIT. A portion of this work was performed at the National High Magnetic Field Laboratory, which is supported by National Science Foundation Cooperative Agreement No. DMR-1157490, the State of Florida, and the US Department of Energy. We acknowledge the National Institute of Standards and Technology, US Department of Commerce, in providing the BT-7 neutron facility used in this work.

Author contributions

T.S. and Y.-T.L. synthesized the crystals. T.S., A.D. and Y.-T.L. performed the electrical measurements. T.S., R.C. and J.W.L. performed the neutron scattering experiments. W.F. and D.X. performed the electronic structure calculations. All authors participated in discussion of the results and writing the paper. J.G.C. coordinated the project.

Additional information

Supplementary information is available in the online version of the paper. Reprints and permissions information is available online at www.nature.com/reprints. Correspondence and requests for materials should be addressed to J.G.C.

Competing financial interests

The authors declare no competing financial interests.

Methods

Single crystals of GdPtBi were grown using a flux method following ref. 24. A mixture of 99.99% Pt wire, 99.9% pure Gd, and 99.999% Bi needles in a molar ratio of 1:1:20 was put in an alumina crucible and sealed in an evacuated quartz tube with 0.016 MPa Argon gas. The sample was heated at 1,100 °C for 2 h and then cooled slowly between 900 °C and 600 °C at a rate of 2 °C h^{-1}, followed by centrifuging to dissociate the GdPtBi crystals from the Bi flux. For neutron scattering experiments, 97.7% isotope-enriched ^{160}Gd (with a purity of 99.9%) was used. All the obtained crystals were confirmed to be of single phase by a powder X-ray diffraction method. The crystals were aligned by X-ray Laue back-reflection and/or single-crystal X-ray diffraction techniques. Transport measurements were performed with a conventional four-probe method. To correct for contact misalignment, the measured longitudinal and transverse voltages were field symmetrized and antisymmetrized, respectively. Magnetization measurements were performed using a commercial superconducting quantum interference device (SQUID) magnetometer. Torque magnetometry was performed using a BeCu cantilever, with the deflection detected by a capacitance bridge. Neutron scattering measurements were carried out on the triple-axis spectrometer BT-7 at the NIST Center for Neutron Research[41]. Electronic structure calculations were performed using the projector augmented wave method and exchange–correlation potential with the generalized gradient approximation of Perdew–Burke–Ernzerhof parameters, implemented in the Vienna *ab initio* simulation package[42].

Data availability. The data that support the plots within this paper and other findings of this study are available from the corresponding author upon reasonable request.

References

41. Lynn, J. W. *et al*. Double-focusing thermal triple-axis spectrometer at NCNR. *J. Res. Natl Inst. Stand. Technol.* **117,** 61–79 (2012).
42. Kresse, G. & Furthmuller, J. Efficient iterative schemes for *ab initio* total-energy calculations using a plane-wave basis set. *Phys. Rev. B* **54,** 11169–11186 (1996).